









## Letter

# L–H transition threshold studies in helium plasmas at JET

E.R. Solano<sup>1</sup> , G. Birkenmeier<sup>2,3</sup> , E. Delabie<sup>4</sup>, C. Silva<sup>5</sup> , J.C. Hillesheim<sup>6</sup>, A. Boboc<sup>6</sup>, I.S. Carvalho<sup>5</sup>, P. Carvalho<sup>5</sup>, M. Chernyshova<sup>7</sup>, T. Craciunescu<sup>8</sup>, E. de la Luna<sup>1</sup>, J.M. Fontdecaba<sup>1</sup> , R. Henriques<sup>5</sup>, P. Jacquet<sup>6</sup>, I. Jecu<sup>8</sup>, A. Kappatou<sup>3</sup> , D. King<sup>6</sup>, M. Lennholm<sup>6</sup>, E. Lerche<sup>9</sup>, E. Litherland-Smith<sup>6</sup>, A. Loarte<sup>10</sup> , M. Maslov<sup>6</sup>, F. Parra Diaz<sup>11</sup>, V. Parail<sup>6</sup>, E. Pawelec<sup>12</sup> , F.G. Rimini<sup>6</sup>, A. Shaw<sup>6</sup>, P. Siren<sup>6</sup>, G. Szepesi<sup>6</sup>, Z. Stancar<sup>13</sup>, E. Tholerus<sup>6</sup> , S. Vartanian<sup>14</sup>, B. Viola<sup>6</sup>, H. Weisen<sup>15</sup> and JET Contributors<sup>a</sup>

<sup>1</sup> Laboratorio Nacional de Fusión, CIEMAT, Madrid, Spain

<sup>2</sup> Physik-Department E28, Technische Universität München, 85748 Garching, Germany

<sup>3</sup> Max-Planck-Institut für Plasmaphysik, D-85748 Garching, Germany

<sup>4</sup> Oak Ridge National Laboratory, Oak Ridge, TN 37831-6169, TN, United States of America

<sup>5</sup> Instituto de Plasmas e Fusão Nuclear, Instituto Superior Técnico, Universidade de Lisboa, Portugal

<sup>6</sup> CCFE, Culham Science Centre, Abingdon, Oxon, OX14 3DB, United Kingdom of Great Britain and Northern Ireland

<sup>7</sup> Institute of Plasma Physics and Laser Microfusion, Hery 23, 01-497 Warsaw, Poland

<sup>8</sup> The National Institute for Laser, Plasma and Radiation Physics, Magurele-Bucharest, Romania

<sup>9</sup> Laboratory for Plasma Physics Koninklijke Militaire School, Ecole Royale Militaire Renaissancelaan 30 Avenue de la Renaissance B-1000, Brussels, Belgium

<sup>10</sup> ITER Organization, Route de Vinon, CS 90 046, 13067 Saint Paul Lez Durance, France

<sup>11</sup> Rudolf Peierls Centre for Theoretical Physics, University of Oxford, Oxford OX1 3PU, United Kingdom of Great Britain and Northern Ireland

<sup>12</sup> Institute of Physics, Opole University, Oleska 48, 45-052 Opole, Poland

<sup>13</sup> Slovenian Fusion Association (SFA), Jozef Stefan Institute, Jamova 39, SI-1000 Ljubljana, Slovenia

<sup>14</sup> CEA, IRFM, F-13108 Saint Paul Lez Durance, France

<sup>15</sup> Ecole Polytechnique Fédérale de Lausanne (EPFL), Swiss Plasma Center (SPC), CH-1015 Lausanne

E-mail: [emilia.solano@ciemat.es](mailto:emilia.solano@ciemat.es)

Received 15 July 2021, revised 3 September 2021

Accepted for publication 29 September 2021

Published 22 October 2021



CrossMark

## Abstract

We present a study of the power threshold for L–H transitions ( $P_{LH}$ ) in almost pure helium plasmas, obtained in recent experiments at JET with an ITER-like wall (Be wall and W divertor). The most notable new result is that the density at which  $P_{LH}$  is minimum,  $\bar{n}_{e,min}$ , is

\* Author to whom any correspondence should be addressed.

<sup>a</sup> See Joffrin *et al* 2019 (<https://doi.org/10.1088/1741-4326/ab2276>) for the JET Contributors.



Original content from this work may be used under the terms of the [Creative Commons Attribution 4.0 licence](https://creativecommons.org/licenses/by/4.0/).

Any further distribution of this work must maintain attribution to the author(s) and the title of the work, journal citation and DOI.

considerably higher for helium than for deuterium and hydrogen plasmas. We discuss the possible implications for ITER in its pre-fusion operating power phase.

Keywords: helium, L–H transition, tokamak

(Some figures may appear in colour only in the online journal)

## 1. Introduction

Characterizing and understanding the L–H transition [1], and especially its power threshold, is a major goal of various L–H transition experiments [2–4] undertaken in JET since the installation of the ITER-like-wall (JET-ILW). Since the JET-ILW campaigns started, we have reported on results of L–H transition studies in hydrogen (H, protium), deuterium (D), H + D mixtures [2, 3] and H + helium mixtures [4]. In this contribution we report on results from L–H transitions studies in almost pure <sup>4</sup>helium (<sup>4</sup>He) plasmas, and additional D plasmas developed to match the densities of the He plasmas obtained and provide the appropriate context for comparative studies.

The interest on He plasmas is not purely academic. The ITER research plan includes a low toroidal field pre-fusion operating power phase with either hydrogen or helium plasmas in order to study H-modes as early as possible, before neutron activation takes place in D plasmas. A prediction of the electron density,  $n_e$ , at which the power required to enter H-mode is minimal,  $\bar{n}_{e,\min}$ , is made inspired on the studies of Ryter *et al* [5] and recently described in more detail in [6], postulating that a critical ion heat flux across the separatrix is necessary to achieve sufficient radial electric field. Assuming pure electron heating in ITER,  $\bar{n}_{e,\min}$  has been evaluated on the basis of 1.5-D transport modelling as the density at which the edge ion power flux starts to saturate with increasing density. The resulting prediction for ITER is that  $\bar{n}_{e,\min} \sim 0.4 \times n_{e,\text{GW}}$ , independent of the ion species [7]. The transition condition in the ITER model depends on two assumptions: (a) the He power threshold,  $P_{\text{LH}}(\text{He})$ , is  $1.4 \times P_{\text{LH}}(\text{D})$ , as found in JET with a carbon wall, JET-C [8]; and (b)  $P_{\text{LH}}(\text{H}) = 2 \times P_{\text{LH}}(\text{D})$ . We show here that JET-ILW results are not so simple: there is a clear change in  $\bar{n}_{e,\min}$  as the plasma species changes.

## 2. Experiment design, definitions

We carried out experiments in helium that could be matched with existing datasets. At medium field, 2.4 T, we can compare D and He, while at low field, 1.8 T, we can compare H, D, and He. In JET-ILW the plasma shape affects the L–H threshold [9, 10], so two different shapes were studied at low field.

To ensure minimal contamination of the helium plasmas in our study, 18 plasma pulses preceding the L–H transition experiments were taken with only helium gas injection (no injection of hydrogenic species). In those pulses  $Z_{\text{eff}} = 2 \pm 0.05$ . These preceding pulses were used for cali-

bration of various spectroscopic measurements, in preparation for the tritium and DT campaigns at JET. Throughout the calibration pulses and the L–H transition pulses, the divertor cryopump operated as usual, removing any recycled hydrogenic species. No argon frosting was used to pump helium.

In this article, helium concentration is defined as the density of helium divided by electron density,  $c_{\text{He}} = n_{\text{He}}/n_e$ , and in a pure helium plasma would be 0.5 or 50%. A derived, more intuitive, quantity is the helium fraction: the ratio of helium density to main ion density  $f_{\text{He}} = n_{\text{He}}/(n_{\text{He}} + n_{\text{H}} + n_{\text{D}})$ . Which is 1 or 100% for a pure helium plasma. Details of He concentrations measurements are provided in section 5. An effective mass is computed adding the contributions from H, D and He in each case, ignoring impurities.

As is well known,  $n_{e,\text{GW}}[10^{20} \text{ m}^{-3}] = I_p[\text{MA}]/\pi(a[\text{m}])^2$  is the Greenwald limit density [11]. The fraction  $f_{\text{GW}} = n_e/n_{e,\text{GW}}$  provides a convenient measure of density for extrapolation studies. The line averaged electron density,  $\bar{n}_e$ , is used throughout this manuscript.

As usual in L–H transition studies, power ramps were used to identify  $P_{\text{loss}} = P_{\text{aux}} + P_{\text{Ohm}} - dW/dt$  at the time of the L–H transition. The ramps were typically  $1 \text{ MW s}^{-1}$ , slow enough that  $dW/dt < 0.5 \text{ MW}$  before the L–H transition. The L–H transition power threshold can be characterized by  $P_{\text{loss}}$ , or by the power across the separatrix, defined as  $P_{\text{sep}} = P_{\text{loss}} - P_{\text{rad}}$ , where  $P_{\text{rad}}$  is the bulk plasma radiation, inside of  $\Psi_N = 0.95$ , where  $\Psi_N$  is the normalised toroidal flux. In most cases we smooth input power, plasma energy and radiation with a time constant of 235 ms, as done in earlier JET L–H transition studies, and most quantities are averaged over the 70 ms prior to the transition. To avoid contamination of the  $dW/dt$  term with post-transition evolution of  $W_{\text{dia}}$ ,  $dW/dt$  is taken a further 100 ms earlier. But when sudden NBI blips cause the transition (see section 4) we must correct  $dW/dt$  and take shorter averages to characterise the power threshold correctly. Since NBI blips typically last 50 ms, we chose 30 ms averaging of unsmoothed quantities to characterise the power terms. We do not display error bars: they can typically be gleaned from the scatter in the data. Systematic errors are of order 10%.

## 3. L–H transition experiments in helium plasmas: medium field D-NBI heating

A density scan was carried out in helium plasmas with 2.4 T toroidal field and 2 MA plasma current, with  $q_{95} = 3.7\text{--}3.9$ . These plasmas were heated by deuterium neutral beam injection (D-NBI).

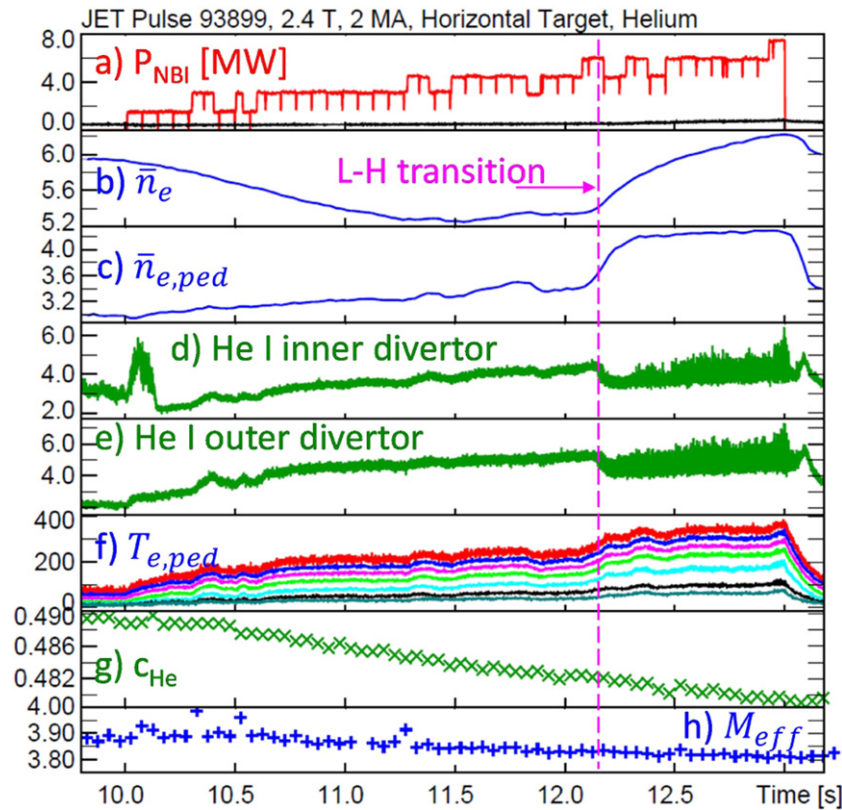


**Figure 1.** Time traces of L–H transition in helium plasma with NBI heating, JET #93 899. (a) NBI injected power in red and radiated power inside 0.95 in black. (b) Line averaged electron density,  $\bar{n}_e$ ; (c) pedestal line averaged density  $\bar{n}_{e,ped}$  (d) He I light, inboard divertor, (e) He I light, outboard divertor, (f) electron temperature ( $T_e$ ) channels, (g) helium concentration, (h) effective ion mass.

Shown in figure 1 are relevant time traces of one of these helium plasma pulses, with the L–H transition time marked by a vertical dashed line. It shows that plasma density before the transition was reasonably controlled by the feedback system, and although the He concentration decreases as D–NBI increases we find that  $f_{He} = 0.93$  at this L–H transition.

Shown in figure 2 is  $P_{loss}$  as a function of line averaged density (lower horizontal axis) and  $f_{GW}$  (upper horizontal axis). There are two notable features in this dataset: (a) L–H transitions are obtained in He up to 90% of Greenwald density and (b) there is a strong shift towards higher density of the density at which  $P_{loss}$  is minimum,  $\bar{n}_{e,min}$  from about  $f_{GW} = 0.41$  in D to 0.64 in He, a 50% increase. Not at all what was expected for ITER: experimental studies in AUG [12] and ITER simulations [7] report the same  $\bar{n}_{e,min}$  in D and He (observed and expected, respectively). Figure 3 shows the corresponding  $P_{sep}$  values as a function of density.

It is notable that both  $P_{loss}$  and  $P_{sep}$  of D and He have very similar values above  $\bar{n}_{e,min}(He)$ , both comparable but below the 2008 ITPA scaling law. The multi-device 2008 ITPA scaling law [13] was constructed with  $P_{loss}$  information, without subtracting radiation, but instead selecting only plasmas with  $P_{rad}/P_{loss} < 0.5$ .

All of these L–H transitions took place with high helium fraction. The next most abundant species was deuterium from the NBI injection. The pulse with highest power threshold, at the lowest density, had a transition at the end of the ramp, with

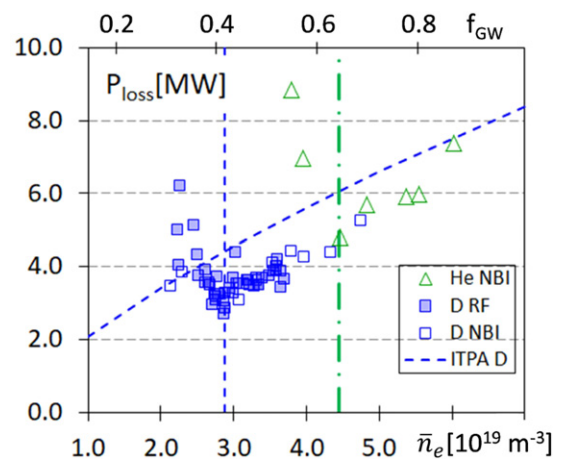


**Figure 2.**  $P_{loss}$  as a function of average electron density (lower horizontal axis) and Greenwald fraction (upper horizontal axis) for deuterium RF and NBI heated plasmas and helium D–NBI heated plasmas.

92% He fraction, the lowest one in this dataset. In the conventional expectation that the  $P_{LH}(He) \geq P_{LH}(D)$ , the D contamination might lower  $P_{LH}$ , and therefore cannot explain why the power threshold increases below  $\bar{n}_{e,min}(He) = 4.4 \times 10^{19} \text{ m}^{-3}$ . All these plasmas classify as helium plasmas with some deuterium contamination.

When D–NBI is used to heat the He plasma, the active charge-exchange diagnostics can in principle provide ion

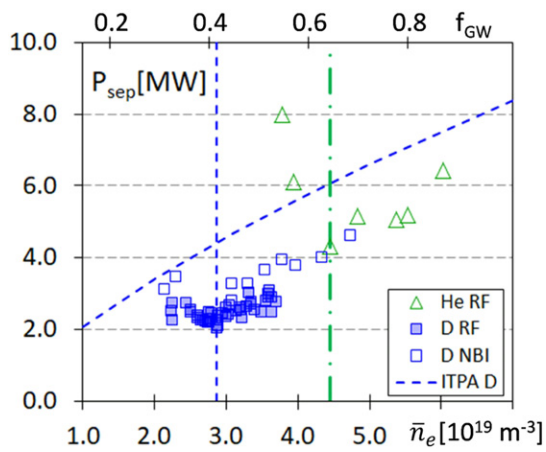


**Figure 3.**  $P_{\text{sep}}$  as a function of average electron density (lower horizontal axis) and Greenwald fraction (upper horizontal axis) for deuterium RF and NBI heated plasmas and helium D-NBI heated plasmas.

temperature, rotation ( $T_i$ ,  $V_{\text{tor}}$ ) and helium concentration measurements. Alas, different spectrometers produce somewhat different  $T_i$  profiles, and helium plume effects have not been corrected for yet [14], so we can not yet present these measurements. Nevertheless, power balance analysis with JETPEAK [15] and TRANSP [16] both indicate that  $T_i \cong T_e$ , even at the lowest densities sampled in the D-NBI heated helium plasmas.

Measurements of the propagation velocity of edge fluctuations with Doppler reflectometry [17, 18] are available for these medium field pulses. They are discussed in the accompanying paper by Silva *et al* [19]. Unfortunately the edge CX measurements were not calibrated for rotation measurements in helium, so we cannot report on edge rotation before and after the transition.

#### 4. L–H transition experiments in helium with ICRH (low field)

Radio-frequency (RF) wave heating was selected for L–H transition experiments with  $B_{\text{tor}} = 1.8$  T, 1.7 MA,  $q_{95} = 3.3$ –3.5. The heating scheme in He and D plasmas was ion cyclotron resonance heating (ICRH) of a hydrogen minority (typically  $n_{\text{H}}/n_e < 5\%$ ), 1st harmonic resonance, 33 MHz, resonant at 2.46 m, inboard of the magnetic axis at  $\sim 3$  m, outside the inversion radius, which in these pulses was at 2.63 m inboard and 3.25 m outboard.

For H plasmas 51 MHz hydrogen majority heating was used, resonant at  $R = 3.19$  m, outboard of the magnetic axis, just inboard of the inversion radius. In both cases off-axis deposition ensures small, frequent sawteeth, which is a beneficial situation for L–H transition studies, since often sawtooth arrival at the edge can trigger transitions.

In most pulses there were two ICRH power ramps, one with the outer strike line at the horizontal target, abbreviated as HT, one with the strike lines in the divertor ‘corners’, corner shape, abbreviated as CC. Both plasma shapes are shown in figure 4, they almost only differ in the divertor region.

Blips of D-NBI heating were added at the end of each RF ramp while RF is held constant, as shown in figure 5. Typically the first NBI blip provided 1.3 MW for 50 ms, the 2nd blip 2.6 MW for 50 ms. Often RF power alone proved to be insufficient to investigate  $P_{\text{LH}}$  as a function of density and transitions took place during the NBI blips. Because the blips produce a faster power ramp than the underlying  $1 \text{ MW s}^{-1}$  of the ICRH ramp,  $dW/dt$  and  $P_{\text{rad}}$  are averaged over a shorter time than usual for L–H transition studies at JET (30 ms instead of 70 ms). The D-NBI-aided transitions are necessarily short lived, providing at best a lower bound for  $P_{\text{loss}}$  and  $P_{\text{sep}}$ , since we cannot discard the need for higher input power for the plasma to remain in H-mode after the short blips. Only in a few cases the available RF power was sufficient to trigger an L–H transition in helium plasmas, marked in the plots with green triangles.

##### 4.1. HT at 1.8 T

As shown in figures 6 and 7, in the HT shape we observe the already reported shift in  $\bar{n}_{e,\text{min}}$  for hydrogen plasmas relative to deuterium [10], and now a further shift for helium: from  $f_{\text{GW}}$  of 0.37 in D, to 0.48 in H and 0.59 in He, a 60% shift between D and He.

In terms of  $P_{\text{loss}}$  required to obtain L–H transitions, shown in figure 6, H and He are globally similar. The difference in threshold power between NBI heating and RF heating in hydrogen plasmas has been noted before [20], but the lack of good rotation measurements preclude detailed interpretation. When radiated power is subtracted He appears to be more attractive (especially at higher densities), as shown in figure 7:  $P_{\text{sep}}(\text{He})$  is significantly lower than  $P_{\text{sep}}(\text{H})$ . In terms of  $P_{\text{sep}}$ , in the high density branch He and D have similar threshold powers, lower than but approximately aligned with the ITPA 2008 scaling, while for hydrogen  $P_{\text{sep}}$  displays a higher power threshold. This is in part due to the large bulk radiation associated with H-minority RF heating in these largely RF-heated He plasmas.

In terms of minimum auxiliary power required to obtain an L–H transition at each  $\bar{n}_{e,\text{min}}$ : 4.5 MW of RF were required in H, 1 MW of RF in D, and 4.7 MW of RF in He.

##### 4.2. Corner shape at 1.8 T

The corner shape typically has a higher power threshold than HT for medium densities, and it is rarely possible to identify  $\bar{n}_{e,\text{min}}$ . Because of the overall higher threshold, this plasma shape could not be studied in hydrogen with RF heating alone, and most of the data points in all species/isotopes had mixed heating. As in HT, the mixed heating points in He are a lower bound of the threshold powers, since NBI blips only last a short time. This is not so for the hydrogen and deuterium points, in which power ramps were constructed combining RF heating ramps with constant D-NBI in D, and combined RF and H-NBI ramps in H.

Shown in figures 8 and 9 are plots of threshold  $P_{\text{loss}}$  and  $P_{\text{sep}}$  for the corner shape. Marked with upward black arrows are datapoints with very marginal transitions: the threshold is

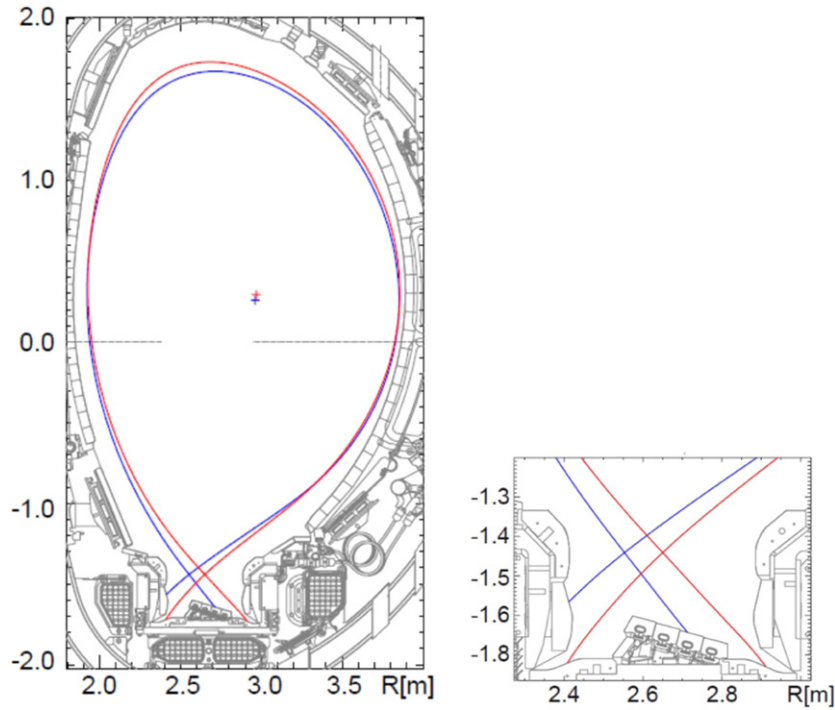


**Figure 4.** Plasma shapes investigated in this study. HT in blue, corner (CC) in red.

higher. Here we see that the  $\bar{n}_{e,\min}$  of helium is quite flat, but can be identified near  $f_{GW} = 0.45$ . Deuterium may have it near or below  $f_{GW} = 0.3$ – $0.4$ , but it is difficult to be sure. At the lowest density, the  $P_{\text{sep}}$  of helium is about 2–3 times the  $P_{\text{sep}}$  of deuterium. At high density  $P_{\text{sep}}$  for He and D are quite similar, and they are both near the deuterium ITPA 2008 prediction. For this plasma shape helium has lower  $P_{\text{loss}}$  than H for  $f_{GW} > 0.4$ , but large radiation in low density He plasmas is subtracted from  $P_{\text{sep}}$ , so in terms of  $P_{\text{sep}}$  He exhibits a lower L–H threshold than hydrogen for almost all cases. Still, we must remember that in helium, unlike in H and D, for all helium plasmas with transitions during NBI blips we are plotting a lower bound of  $P_{\text{sep}}$ , the power threshold for a steady H-mode in He might be higher.

The minimum auxiliary power input required to obtain a transition in the corner shape was 7 MW in H (mixed RF + NBI), 2.3 MW (mixed heating) in D and 4.9 MW (pure RF heating) in He.

### 5. Helium diagnostics, concentration measurements

Measurements of He concentration  $c_{\text{He}} = n_{\text{He}}/n_e$  in the neutralized particle exhaust in the JET sub-divertor region were carried out with an optical penning (or species-selective penning) Gauge, as described in [21]. By the time the L–H transition experiments began,  $f_{\text{He}}$  was at least 0.85 (lowest density point in corner shape), and in most cases  $f_{\text{He}} > 0.92$ . Assuming the rest of the plasma to be composed of hydrogenic species, the implication is that at most 8% of the plasma ions were hydrogenic in any of the L–H transitions presented here.

TRANSP interpretive analysis of D-NBI heated He background L–H transition pulses was undertaken to correlate the neutron measurements (dominated by beam–target and beam–beam DD reactions) with the spectroscopic deuterium concentration measurements. Prescribed  $n_D$  profiles were used, scaling a constant  $n_D/n_e$  profile from the spectroscopic measurements at the edge. Assuming  $T_i = T_e$ , we obtain agreement with the spectroscopic measurement of D concentration at medium-high density (93 898,  $f_{GW} = 0.7$ ) matching the measured neutron rate. If lower  $T_i$  is assumed, the D concentration required to meet the neutron rate rises accordingly. The variations fall well within the 10% error bars of the neutron measurement. Therefore this TRANSP analysis gives us confidence in using edge spectroscopic measurements to characterise He concentration in the plasma core.

### 6. Discussion and summary

The JET-ILW L–H transition results show a larger shift in  $n_{e,\min}$  between D and He plasmas than previously reported anywhere. Our results in the HT shape clearly indicate different values for  $n_{e,\min}$  for H, D and He, already described. Remarkably, despite the differences in  $I_p$  in our datasets,  $\bar{n}_{e,\min}$  can be described in terms of the Greenwald density:

$$\bar{n}_{e,\min}(\text{D}) = 0.4 \times n_{GW}$$

$$\bar{n}_{e,\min}(\text{H}) = 0.5 \times n_{GW}$$

$$\bar{n}_{e,\min}(\text{He}) = 0.6 \times n_{GW}.$$

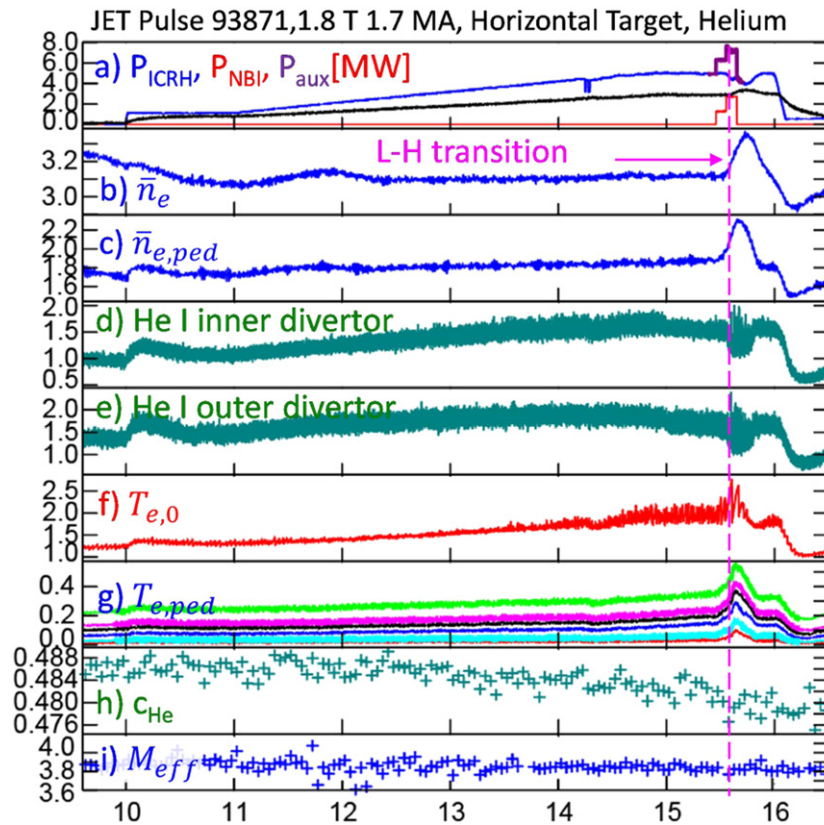


**Figure 5.** Time traces of L–H transition in helium plasma with RF heating and NBI blips, JET #93 871. (a) RF power in blue, NBI blips in red, total  $P_{\text{aux}}$  in purple radiated power inside 0.95 in black. (b) Line averaged electron density,  $\bar{n}_e$ , (c) pedestal line averaged density  $\bar{n}_{e,\text{ped}}$ , (d) He I light, inboard divertor, (e) He I light, outboard divertor, (f) core electron temperature  $T_e$ , (g)  $T_e$  edge channels, (h) helium concentration, (i) effective ion mass.

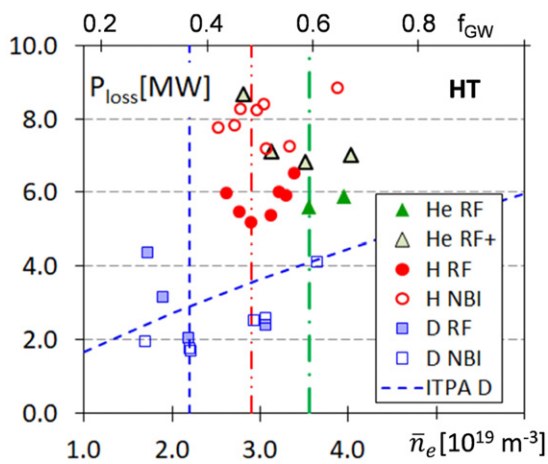


**Figure 6.**  $P_{\text{loss}}$  at the L–H transition as a function of  $\bar{n}_{e,\text{av}}$  (lower horizontal axis) and  $f_{\text{GW}}$  (upper horizontal axis) for hydrogen, deuterium and helium HT plasmas. The green triangle symbols correspond to pure RF L–H transitions, ones with a black boundary have added NBI blips. Dashed blue line indicates 2008 ITPA deuterium scaling. Coloured vertical lines mark  $\bar{n}_{e,\text{min}}$  for each species.

The situation in the corner shape appears to be similar, with  $\bar{n}_{e,\text{min}}(\text{He}) \cong 0.4 \times n_{\text{GW}}$  and presumably near or below  $0.3 \times n_{\text{GW}}$  for H and D, as usual lower than for the HT shape.

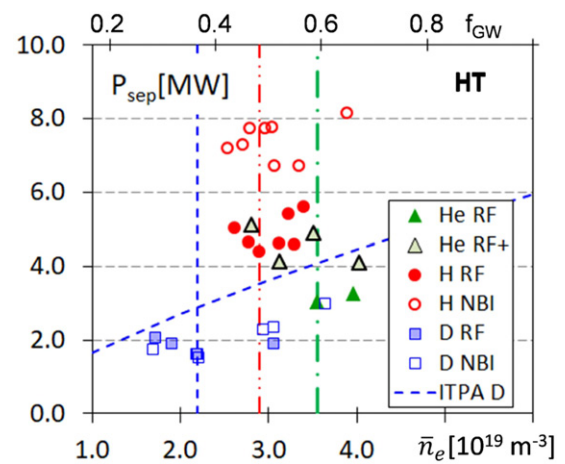


**Figure 7.**  $P_{\text{sep}}$  values for HT plasmas corresponding to figure 6.

In the HT shape, above  $\bar{n}_{e,\text{min}}$ ,  $P_{\text{sep}}$  in JET-ILW is similar for D and He, and near or below the 2008 ITPA scaling. Therefore the increase in the predicted  $P_{\text{sep}}(\text{He})$  due to higher  $\bar{n}_{e,\text{min}}(\text{He})$  is compensated by the lower overall power required to access it, since ITER had assumed  $P_{\text{LH}}(\text{He}) = 1.4 \times P_{\text{LH}}(\text{D}) \sim 2008$  ITPA. In the corner shape  $P_{\text{sep}}(\text{deuterium})$  is near the ITPA 2008, while  $P_{\text{sep}}(\text{He})$  is somewhat higher. Overall we observe that  $P_{\text{sep}}(\text{He}) \sim P_{\text{sep}}(\text{D})$  at sufficiently high density,

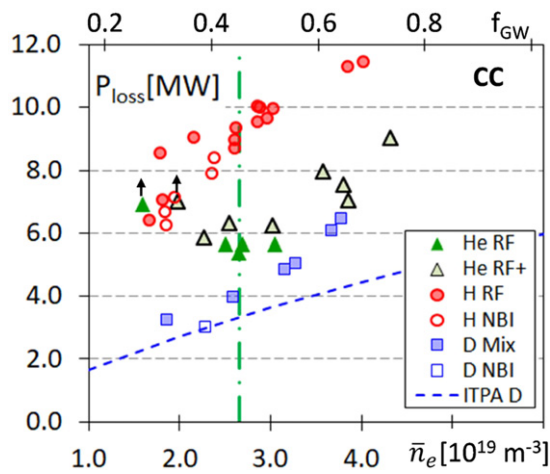


**Figure 8.**  $P_{\text{loss}}$  as a function of  $n_{e,\text{av}}$  and  $f_{\text{GW}}$  (upper horizontal axis) for H, D and He corner plasmas.

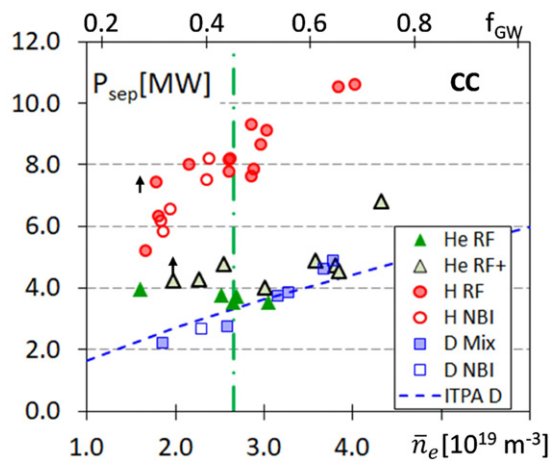


**Figure 9.**  $P_{\text{sep}}$  values for corner plasmas, as in figure 8.

while  $P_{\text{loss}}(\text{He})$  at  $\bar{n}_{e,\text{min}}(\text{He})$  is comparable to  $P_{\text{loss}}(\text{H})$  at  $\bar{n}_{e,\text{min}}(\text{H})$  in the HT shape. We compare  $P_{\text{sep}}$  to the ITPA scaling law despite the fact that it was constructed without subtracting radiation because the expectation in ITER is that impurity content and radiation will be low, and therefore a prediction of  $P_{\text{loss}}$  would be equivalent to a prediction of  $P_{\text{sep}}$ .

Earlier JET results, with graphite plasma facing components, have reported  $P_{\text{LH}}(\text{He}) \sim 1.4 \times P_{\text{LH}}(\text{D})$  [8, 22]. They were obtained from assuming the ITPA 2008 scaling law has the correct dependency for He and D. Carrying out a fit of the He L–H transition data to the scaling law provided the 1.4 multiplier for He  $P_{\text{LH}}$  compared to D, mixing data from different fields and currents, and probably mixing high and low density branches, unidentified at the time. For instance, for the 1.8 T, 1.7 MA, HT JET-C dataset there was very little overlap on densities between He and D plasmas (see figure 3 of reference [22]). Here we have data rather than scaling laws, and we find about the same  $P_{\text{sep}}$  for He and D in the experimentally identified high density branch of He.

Questions do remain about the scaling of radiation as a function of species. We show in figure 10 the bulk radiation

at the L–H transition as a function of plasma species and electron density for the three datasets presented earlier. In the HT shape (figures 10(a) and (b)) the highest radiation points correspond to densities below  $\bar{n}_{e,\text{min}}$ , both in D and He, especially with RF heating. At low field (figures 10(b) and (c)), between  $3$  and  $4 \times 10^{19} \text{ m}^{-3}$  radiation is almost always highest in He, while for higher densities  $P_{\text{rad}}$  appears to align for D and He. Typically H plasmas radiate the least. This is consistent with the lower expected lower W sputtering yield of H vs D and He.

And how do our results compare to those of other devices? DIII-D results at  $I_p = 1.0 \text{ MA}$ ,  $B_T = 1.65 \text{ T}$ ,  $q_{95} = 4.1$  show a  $\sim 20\%$  increase in  $\bar{n}_{e,\text{min}}$ , from  $\bar{n}_{e,\text{min}}(\text{D}) = 0.33 \times n_{\text{GW}}$  to  $\bar{n}_{e,\text{min}}(\text{He}) = 0.4 \times n_{\text{GW}}$  [23]. C-Mod results [24] at  $5.4 \text{ T}$ ,  $0.9 \text{ MA}$ ,  $q_{95} \sim 3.65 \rightarrow 3.9$ , report a 40% shift, from  $\bar{n}_{e,\text{min}}(\text{D}) = 0.17 \times n_{\text{GW}}$  to  $\bar{n}_{e,\text{min}}(\text{He}) = 0.24 \times n_{\text{GW}}$ . Both are in qualitative agreement with our observation that  $\bar{n}_{e,\text{min}}$  is significantly higher for He than for D, although the actual values of the  $\bar{n}_{e,\text{min}}$  vary. Variability on the values of  $\bar{n}_{e,\text{min}}$  across devices is to be expected. For instance it is already known that even in the same device lowering  $I_p$  reduces  $\bar{n}_{e,\text{min}}$  [10, 12], and that plasma shape in the divertor region can strongly impact both  $P_{\text{LH}}$  and  $\bar{n}_{e,\text{min}}$  [9, 10, 25].

The exception is AUG, where studies report little or no difference in  $\bar{n}_{e,\text{min}} \sim 0.35 \times n_{\text{GW}}$  between H, D and He, and the same  $P_{\text{LH}}$  for D and He [12, 26]. The dataset described is complex, as plasmas with different  $B_T$  and  $I_p$  are sometimes compared with each other via renormalization of the  $B_t$  dependency. Understanding why the AUG results are different to others requires detailed analysis of the AUG data beyond the scope of this report on JET-ILW results.

Overall, the JET datasets presented here encompass a wider density range for all species than all those previously reported, clearly documenting high power thresholds in He at lower densities.

We believe the L–H transition power threshold is defined by the plasma transport characteristics in L-mode, and it is possible that they depend on species, density, shape, size and fields in non-linear ways. Density or density gradient in L-mode, and maybe their relation to temperature gradients, as well as plasma mass and charge are likely to control the type of instabilities present in the plasma [27] and therefore affect the transport and L–H threshold. Analysis of such detailed physics models far exceeds the objectives of the experimental study presented here. Much of it will only be possible with ion profile information.

Nevertheless, following up on the insights of earlier work, mostly in deuterium, we can make some comments. First, rotation (unmeasured here) is unlikely to explain the shift in  $\bar{n}_{e,\text{min}}$ , because similar shifts are obtained in RF heated (no momentum input) and co-injected NBI heated plasmas (with momentum input). Secondly, on the explanations of  $\bar{n}_{e,\text{min}}$  based on electron–ion heat exchange: they largely originate in studies of electron heated plasmas [5, 6, 24], with low rotation, and our heating methods typically produce at least 50% ion heating (in D plasmas), so they may not apply. Further, sufficiently large deuterium contamination or a non-linear dependence of the power threshold on plasma composition [4, 23], could affect

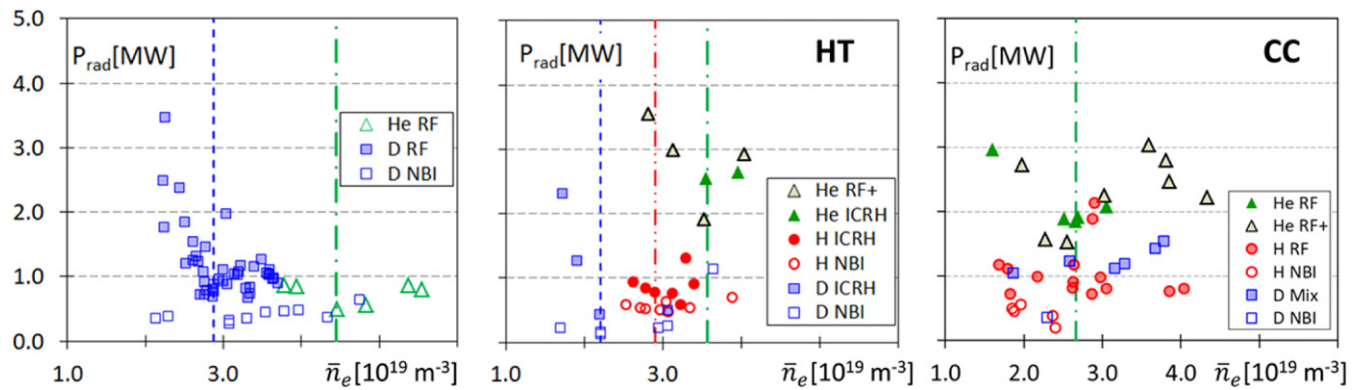


**Figure 10.** Bulk radiation  $P_{\text{rad}}$  corresponding to the transitions depicted in (a) 2.4 T 2.0 MA HT, figures 2 and 3; (b) 1.8 T 1.7 MA HT, figures 6 and 7; (c) 1.8 T 1.7 MA CC, figures 8 and 9.

$\bar{n}_{e,\text{min}}$  differently in different experiments. In our case we find that D contamination in the low density branch of He plasmas might mask a larger shift, rather than explain the shift observed.

In terms of the L–H transition, our HT results raise questions about the logic that supports He for access to H-mode in the early operating phase of ITER but not about the final estimate, as long as  $P_{\text{rad}}$  in ITER helium plasmas is not very large.

## Acknowledgments

This work has been carried out within the framework of the EUROfusion Consortium and has received funding from the Euratom research and training programme 2014–2018 and 2019–2020 under Grant Agreement No. 633053. The views and opinions expressed herein do not necessarily reflect those of the European Commission. Additionally, this work was supported in part by the Spanish National Research Plan, FEDER/Ministerio de Ciencia, Innovación y Universidades—Agencia Estatal de Investigación/Proyecto FIS2017-85252-R

## ORCID iDs

E.R. Solano <https://orcid.org/0000-0002-4815-3407>  
 G. Birkenmeier <https://orcid.org/0000-0001-7508-3646>  
 C. Silva <https://orcid.org/0000-0001-6348-0505>  
 J.M. Fontdecaba <https://orcid.org/0000-0001-7678-0240>  
 A. Kappatou <https://orcid.org/0000-0003-3341-1909>  
 A. Loarte <https://orcid.org/0000-0001-9592-1117>  
 E. Pawelec <https://orcid.org/0000-0003-1333-6331>  
 E. Tholerus <https://orcid.org/0000-0002-3262-1958>

## References

- [1] Wagner F. *et al* 1982 *Phys. Rev. Lett.* **49** 1408
- [2] Maggi C.F. *et al* 2018 *Plasma Phys. Control. Fusion* **60** 014045
- [3] Hillesheim J. *et al* 2016 Role of stationary zonal flows and momentum transport for L–H transitions in JET *26th IAEA Fusion Energy Conf. IAEA CN-234* (Kyoto, Japan, 17–22 October 2016) ([https://nucleus.iaea.org/sites/fusionportal/Shared%20Documents/FEC%202016/FEC2016\\_ConfMat\\_Online.pdf](https://nucleus.iaea.org/sites/fusionportal/Shared%20Documents/FEC%202016/FEC2016_ConfMat_Online.pdf))
- [4] Hillesheim J.C. *et al* 2018 Implications of JET-ILW L–H transition studies for ITER *27th IAEA Fusion Energy Conf.* (Gandhinagar, India, 22–27 October 2018) (<https://conferences.iaea.org/indico/event/151/contributions/>)
- [5] Ryter F. *et al* 2014 *Nucl. Fusion* **54** 083003
- [6] Bilato R. *et al* 2020 *Nucl. Fusion* **60** 124003
- [7] ITER Organization 2018 ITER Research Plan within the Staged Approach (Level III - Provisional Version) Report ITER-Report 18-003 1–351
- [8] McDonald D.C. *et al* 2004 *Plasma Phys. Control. Fusion* **46** 519
- [9] Delabie E. 2014 Overview and interpretation of L–H threshold experiments on JET with the ITER-like wall *25th Fusion Energy Conf. (FEC 2014)* (Saint Petersburg, Russia, 13–18 October 2014) ([http://www-naweb.iaea.org/naweb/physics/FEC/FEC2014/fec\\_sourcebook\\_online.pdf](http://www-naweb.iaea.org/naweb/physics/FEC/FEC2014/fec_sourcebook_online.pdf))
- [10] Maggi C.F. *et al* 2014 *Nucl. Fusion* **54** 023007
- [11] Greenwald M. 2002 *Plasma Phys. Control. Fusion* **44** R27–53
- [12] Ryter F. *et al* 2013 *Nucl. Fusion* **53** 113003
- [13] Martin Y.R. *et al* 2008 *J. Phys.: Conf. Ser.* **123** 012033
- [14] Kappatou A. *et al* 2018 *Plasma Phys. Control. Fusion* **60** 055006
- [15] Weisen H. *et al* 2020 *Nucl. Fusion* **60** 036004
- [16] Ongena J.P.H.E. *et al* 2012 *Fusion Sci. Technol.* **45** 371–9
- [17] Hillesheim J.C. 2015 Radial electric field measurements with Doppler backscattering in JET *12th Int. Reflectometry Workshop* (Jülich, Germany, May 2015) (<http://www.aug.ipp.mpg.de/IRW/IRW12/proceedings.html>)
- [18] Silva C. *et al* 2016 *Nucl. Fusion* **56** 106026
- [19] Silva C. *et al* 2021 *Nucl. Fus.* **61** 126006
- [20] Hillesheim J. *et al* 2017 L–H transition studies in hydrogen and mixed ion species plasmas in JET *44th EPS Conf. Plasma Physics* (Belfast, Northern Ireland, UK, 26–30 June 2017) (<http://ocs.ciemat.es/EPS2017PAP/pdf/P5.162.pdf>)
- [21] Vartanian V.S. *et al* 2021 *Fusion Eng. Des.* **170** 112511
- [22] McDonald D. 2010 *23rd Fusion Energy Conf.* (Daejeon, South Korea) (Vienna: IAEA) CD-ROM file [EXC-2-4rb] (<http://naweb.iaea.org/naweb/physics/FEC/FEC2010/index.htm>)
- [23] Gohil P. 2011 *Nucl. Fusion* **51** 103020
- [24] Kessel C.E. *et al* 2018 *Nucl. Fusion* **58** 056007
- [25] Andrew Y. *et al* 2004 *Plasma Phys. Control. Fusion* **46** A87–93
- [26] Ryter F. *et al* 2009 *Nucl. Fusion* **49** 062003
- [27] Bourdelle C. *et al* 2015 *Nucl. Fusion* **55** 073015